Repeatability Precision error analysis of the distributed fiber optic strain monitoring

LINQING LUO[1,2*], YING MEI[3], NICHOLAS DE BATTISTA[4,5], CEDRIC KECHAVARZI[4,5], KENICHI SOGA[2]

[1]*Earth and Environmental Sciences Area, Lawrence Berkeley National Laboratory, 1 Cyclotron Road, MS 74R316C, Berkeley, CA, 94720, USA*
[2]*Department of Civil and Environmental Engineering, University of California, Berkeley, Berkeley, CA 97420, USA*
[3]*Beijing Institute of Aerospace Control Devices, Beijing Engineering Research Center of Optical Fiber Sensing System, No.1 Fengying East Road, Haidian District, Beijing, China, 100094*
[4]*Centre for Smart Infrastructure and Construction, University of Cambridge, Cambridge, UK, CB2 1PZ*
[5]*Epsimon Ltd, UK*
[*]*linqingluo@lbl.gov*

Abstract: The precision error of the Brillouin Optical Time Domain Reflectometry (BOTDR) based distributed fiber optic strain measurement is normally evaluated based on strain change from the initial zero strain state. In many structural health monitoring applications, however, there is initial strain caused by the installation process of a fiber optic sensor cable to a structure. Engineers are interested in the incremental strain profile from the initial strain profile to assess the performance of the structure. The initial strain profile is often not constant throughout the cable length due to the manner that the fiber optic cables are installed (e.g., gluing, clamping, or embedding). This uneven strain distribution causes precision error in the strain incremental values, which in turn leads to difficulty in data interpretation. This paper discusses why large initial strain variation (or initial strain gradient) increases the precision error of the subsequent incremental strain reading and how to evaluate the magnitude of such precision error. A relationship between strain gradient and precision error is demonstrated. A sectional shift method is proposed to minimize the precision error. Results from laboratory tests and a field case study show that the method can reduce the precision error approximately 50% when the strain gradient is large.

Keywords: Distributed fiber optic sensing, structure health monitoring, Error analysis, Noise cancellation, Strain monitoring, Brillouin Optical Time Domain Reflectometry.

1. Introduction

Distributed Brillouin fiber optic sensing has been used for strain and/or temperature monitoring of civil engineering structures[1–4]. Discrete sensors have better spatial resolution and accuracy, whereas the distributed sensors have longer spatial resolution but with worse accuracy[5]. The distributed sensor technologies can solve the issue related to the limitation of sensor numbers and locations on data reliability[6]. However, it can have reduced accuracy and decrease in data repeatability (precision) when compared to highly accurate discrete sensing systems. The sensing repeatability is characterized by the precision error, which is defined by the standard deviation of a number of consecutive measurements [7]. Theoretical and experimental studies have shown that the precision error under zero strain state is fundamentally dependent on the Brillouin gain linewidth, spatial resolution, frequency scanning step, number of averaging times, and signal to noise ratio (SNR) [8,9]. For a typical Brillouin Optical Time Domain Reflectometry (BOTDR) interrogator, its precision error follows a normal distribution with a standard deviation of around 15 με [10] when no strain is applied to the fiber. Under a strained condition, however, the strain measurement of a point loaded beam was reported to have an extra repeatability error of 5 με compared to that of the constant strain condition [11,12].

In many structural health monitoring applications, there is initial strain caused by the installation of a fiber optic sensor cable to a structure. Engineers are interested in the incremental strain profile from the initial strain profile to assess the performance of the

structure. The initial strain profile is often not constant throughout the cable length due to the manner that the fiber optic cable is installed (e.g., gluing, clamping, or embedding). This uneven strain distribution causes precision error in the strain incremental values, which in turn leads to difficulty in data interpretation. In fact, unexpected data fluctuations have been observed and the accuracy of strain and temperature measurement appears to degrade in field applications. For example, the 5-day measurements on the roller compacted concrete (RCC) dam Fundão in Brazil revealed that the precision error was mostly about 70 με along the cable, and up to 500 με at some particular locations (e.g. cable fixation, splice connections and places with local losses) [13]. A maximum precision error of 300 με under fluctuating loads was also reported in a cracked concrete beam when ten repeated measurements were made using BOTDR [14].

These relatively high precision error values are most likely due to the ubiquitous inhomogeneous nature of the real strain field. Non-uniformly distributed strain leads to an asymmetric Brillouin gain spectrum, and thus a lower SNR and broader bandwidth of the received Brillouin spectrum frequency resolution. This is directly related to the frequency resolution of the sensing system [15]. As discussed in this paper, non-uniformity in the initial strain profile can enlarge the distance error in the interrogator acquisition system, which in turn affects the measurement repeatability. The strain range for structural monitoring is commonly limited to several hundreds of micro-strains. Hence, the relatively high precision error caused by the non-uniformity of the initial strain profile could become a critical problem in some applications.

The precision error in this paper is characterized as the combination of frequency error and distance error. The frequency error is a random error in the frequency domain, closely related to the signal to noise ratio, while the distance error is dependent on the timing error of the interrogator's acquisition system. In this study, a method is proposed to quantify the BOTDR frequency and distance resolution induced precision errors. To illustrate the reliability of this method in predicting the magnitude of precision error, comparisons are made between experimental measured error and the predicted error. A relationship between the measured strain gradient and precision error is observed. A precision error compensation method using sectional shift is developed and its performance is evaluated with data sets from laboratory tests and a field pile monitoring case.

2. Precision error

The strain/temperature magnitude, as well as its location recorded by BOTDR/BOTDA systems, are subject to measurement repeatability error, i.e. precision error. The precision error in this paper is defined as the statistical variance of the multiple repeatability readings at each measured location along the sensing cable. The readings are made by using the same instrument and operator while keeping the same loading conditions. It is calculated by taking the standard deviation of multiple readings (about 30-100 readings). The spatial variation of the standard deviation along the sensing fiber can be obtained. Hardware design and implementation influence the precision of measurements; for example, the precision error of the Neubrescope PPP-BOTDA system can be found in paper [16]. The instability of pump and probe laser, the Brillouin gain spectrum's signal to noise ratio (SNR), full width at half maximum (FWHM) and the frequency scanning step influence on the measurement accuracy and repeatability [16]. This study shows that the strain variation on the fiber also contributes to the precision error. The causes of the error can be divided

into the following two: (a) frequency resolution induced error and (b) distance resolution induced error.

2.1 Frequency resolution induced error

Frequency resolution is directly related to the signal noise of an interrogator. As shown in Fig. 1, the measured Brillouin spectrum presents power fluctuations, which make it difficult to evaluate the center frequency of the peak power. In this figure, the center frequency is located in the range of the two dotted lines, which are determined by its frequency resolution. This uncertainty in locating the actual center frequency leads to precision error.

Frequency resolution is partly affected by the optical power of the interrogator. The optical power losses that accumulate along the fiber configuration reduce the SNR in the detection side of the interrogator, especially when power loss happens due to fiber bending. At the same time, the Brillouin spectrum bandwidth also affects the frequency resolution, which is dependent on the SNR and FWHM of the received Brillouin spectrum [17][18]. Previous experimental results verified that the dependency of the Brillouin frequency resolution on measurement parameters can be approximated by the following equation [19]:

$$\delta_{V_f} = \frac{1}{SNR(z)} \sqrt{\frac{3}{4} \phi \cdot \Delta v_B} \tag{1}$$

where SNR is the ratio between peak power and noise, Δv_B is the FWHM of the Brillouin gain spectrum, and ϕ is the frequency step. This equation suggests that the measurement precision error is proportional to the square root of FWHM and inversely proportional to SNR.

When strain change happens spatially, the measured Brillouin spectrums around this location becomes wider as it is a convolution of the intrinsic Brillouin spectra with different peaks over the interrogator's spatial resolution. In this way, the peak region of the Brillouin scattering spectrum becomes flatter. It then becomes difficult to detect the peak, leading to reduction in strain precision. Therefore, when there is a non-uniformly distributed strain profile, the broadening and asymmetry of the Brillouin gain curve affect the frequency resolution of the measurements.

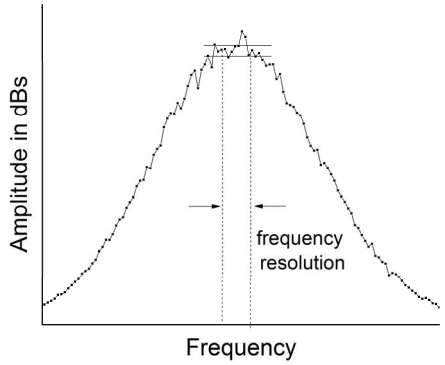

Figure 1 The influence of frequency resolution on strain measurement precision for Brillouin optical time domain system

2.2 Distance resolution induced error

Distance resolution induced error is related to the precision of the spatial location of a measured point (jitter). It is the variance of Brillouin frequency shift due to the uncertainty of the cable location determination inside the interrogator [16]. In optical time-domain based systems, the acquisition scheme (i.e., the sampling rate of the detection system) sets the number points (sampling interval) along the fiber. It corresponds to the localization precision of a measured point with respect to its spatial position.

Distance resolution induced precision error is illustrated in Fig. 2 where three Brillouin spectra represent one measuring point result but have different fiber locations where back scattering occurs due to distance error. When the injected pulse propagates through the fiber, the measured Brillouin spectrum is the convolution of the fiber intrinsic spectrum over the pulse length (interrogator spatial resolution), which is determined by the pulse length. In Fig.2, the convoluted spectrum represents the interrogator measured result. Spectrum 1 and 2 are the intrinsic Brillouin spectra of the fiber over the spatial resolution of the interrogator when a pulse is passing a step change location of two strain sections. When the pulse is half at strain section 1 and half at strain section 2, the intrinsic Brillouin spectra power in these two sections are equally shared, as shown in Fig. 2(a). When the pulse is more at section 1, the power will be dominated by spectrum 1, as shown in Fig 2(b). As a result, the convoluted Brillouin spectrum result deforms. When jitter happens, the center frequency at peak varies for the three measurements, leading to precision error.

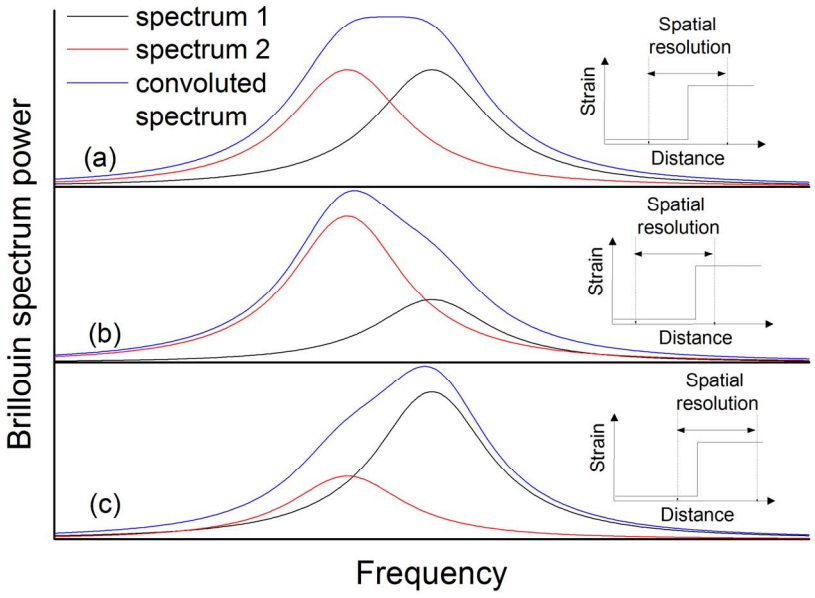

Figure 2 The influence of distance error on strain measurement precision for Brillouin optical time domain system

The amount of distance error induced precision error is dependent on the interrogator's jitter specification as well as the spatial strain change rate (or strain gradient) on the fiber. When the fiber is under no external strain, the distance resolution does not affect the strain readings. However, when the fiber experiences a rapid strain change in space (or large strain gradient), a small error in location determination affects the identification of the peak frequency and hence strain. As a result, the precision error in the strain/temperature

determination increases at locations where there is a large strain change (or the section where the strain gradient is large).

2.3 Precision error in measurements

To demonstrate the aforementioned precision error in measurements, the condition of a sharp strain change was mocked by using a cable spliced by two types of optics fibers, which have a center frequency difference of 500 MHz (equivalent to 1% strain). The first fiber in the cable was mocked as zero strain section and the second fiber in the cable is mocked as strained section. The tested cable was put in free condition and repeated measurements were taken using NBX-5000 BOTDR interrogator (Neubrex). The measured Brillouin center frequency profile was expected to have a step change at the splicing point of the two fibers with different center frequencies. The interrogator was set as 1 m spatial resolution and 0.05 m sampling resolution. 216 measurements were taken and averaged. The recorded Brillouin center frequency profiles were used for the investigation of the frequency resolution induced and distance resolution induced errors.

2.3.1 Frequency resolution

Fig. 3 shows the Brillouin spectrum of the measurement at different strain section locations. Since BOTDR sensor measures a convoluted result over the spatial resolution, the measured Brillouin spectrum at a strain change section contains two peaks; one representing the spectrum at the strained section and the other representing the spectrum at the unstrained section. In this sharp strain change case, the center frequency difference between the strained and unstrained condition is so significant that the double peaks can be clearly seen.

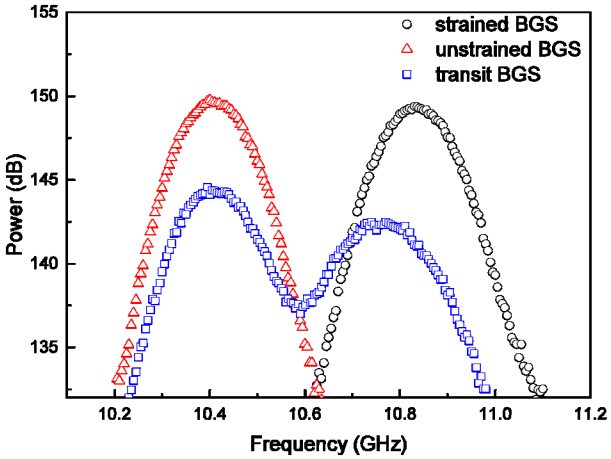

Figure 3 The comparison of Brillouin spectrum at a uniformly strained section, unstrained section and strain transit section

At the strain transient section, the obtained Brillouin gain spectrum becomes distorted compared to that of the uniformly strained section or unstrained section. Because of the sharp frequency change of 500 MHz (red dotted line as the measured Brillouin gain spectrum at the unstrained section and black dotted line as the measured Brillouin gain spectrum at the strained section in Fig. 3), the measured Brillouin spectrum at the strain

change sections shows visible double peaks (blue dotted line). As a result, the SNR is reduced with a lower peak power (assuming the noise level is constant along the cable) and the FWHM increases for the Brillouin gain spectrum at the strain transit section.

According to Eq. 1, a lower SNR and broader FWHM leads to a larger precision error. At rapid strain change sections in Figure 3, the FWHM is enlarged and the SNR is reduced due to the convolution of Brillouin spectra in different peak frequency profiles, resulting in a growth of the precision error. Therefore, the frequency resolution induced precision error can be related to the non-uniformity of the measured strain profile. It is expected that the frequency resolution at strain change section is larger than that at the free cable section, and the increase of the precision error is quantitatively related to the measured gradient of the Brillouin center frequency shift (corresponding to the measured strain gradient).

2.3.1 Distance resolution

To investigate the distance resolution induced precision error, two repeated Brillouin spectrum measurements at the splicing point of the tested cable is compared, as shown in Fig. 4. The power ratio between the two peaks varies with the two measurements: the ratio of the peak power at 10.77 GHz to the peak power at 10.42 GHz is 1.005 for the first measurement and 0.998 for the second measurement. The spectrum peak power is roughly proportional to the length of the event because the measured spectrum is a convolution of the intrinsic Brillouin spectrum over the interrogator's spatial resolution [20]. Therefore, the peak with relatively higher power means that the measuring point is closer to the peak section. The first measurement has a higher power in the strained section, indicating its location is closer to the strained section. The second measurement is the opposite, implying that there is a distance error in measuring point between the two repeated measurements. The final measured center frequency is 10.77 GHz for the first measurement, whereas it is 10.42 GHz for the second measurement. A horizontal shift of the center frequency can be clearly seen, which in turn leads to precision error at the strain change section.

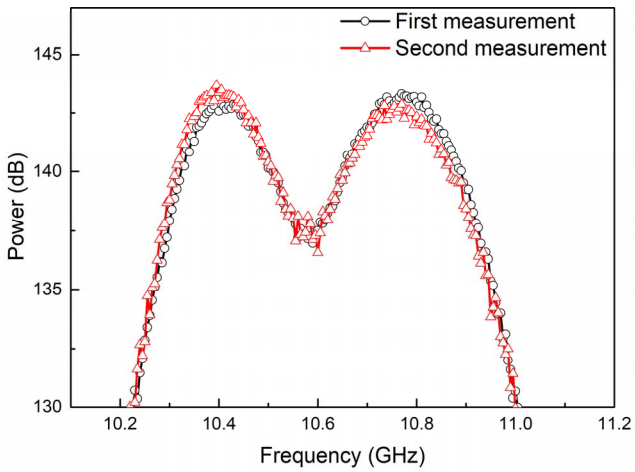

Figure 4 Comparison of two repeated Brillouin spectrum measurements

3. Precision error evaluation

It is important to evaluate the magnitude of precision error in each measurement, especially when long term monitoring is required. The frequency resolution induced error and the distance resolution induced precision error contribute to the precision error. Brillouin measurement frequency resolution ($\delta\nu_f$) can be approximated by Eq. 1. The frequency resolution is dependent on the characteristics of the spectrum and parameter settings of the interrogator. For a typical BOTDR interrogator with an SNR of 20 dB, FWHM of 130 MHz, and frequency scanning step of 3 MHz, the measurement precision error is calculated as 0.8553 MHz using this equation.

To evaluate the distance resolution induced precision error, the interrogator timing error (Δt) first needs to be calibrated in the laboratory. Fig. 5 illustrates the relationship between the interrogator measured precision error ($\delta\nu$) and distance distance resolution (Δz). By subtracting frequency resolution precision error from the interrogator measured precision error, the distance resolution induced precision error can be obtained:

$$\delta\nu_d = \sqrt{\delta\nu^2 - \delta\nu_f^2} \tag{2}$$

where $\delta\nu_d$ is the distance induced precision error, $\delta\nu_f$ is the frequency resolution induced error, and $\delta\nu$ is the measured precision error.

In a short length section, the Brillouin center frequency distribution can be regarded as linearly distributed. If the frequency shift gradient at point z is given as $\Delta\nu_B'(\varepsilon(z))$, the distance resolution induced precision error ($\delta\nu_d$) can be approximated into distance resolution Δz:

$$\Delta z = \frac{\delta\nu_d}{\Delta\nu_B'(\varepsilon(z))} \tag{3}$$

The corresponded timing error (Δt) of the interrogator is calculated as:

$$\Delta t = \frac{\Delta z \times n}{c} \tag{4}$$

where c is the speed of light in vacuum and n is the refractive index of optical fiber.

At a strain change section where there is a large strain gradient $\Delta\nu_B'(\varepsilon(z))$, the distance resolution induced measurement precision error is enlarged, as indicated by Eq. 3. Therefore, the interrogator timing error results in large precision error at the strain change section, similar to the previous frequency resolution effect. Given the interrogator dependent timing error (Δt), the distance resolution induced precision error can be estimated as:

$$\delta\nu_d = \Delta\nu_B'(\varepsilon(z)) \times \frac{\Delta t \times c}{n} \tag{5}$$

A step strain change measurement and its precision were evaluated with NBX-5000 interrogator. In the experiment, the strain-sensing cable was a reinforced-ribbon cable manufactured by Fujikura Ltd. The cores are tightly bonded to the protective nylon sheath for effective mechanical strain transmission. In the test, a section of 1.5 m length reinforced cable (at position 1.1 m and 2.6 m) was strained to 2075 με, whilst the other sections were under the free strain condition. The cable was fixed and strained using a calibration bar. In total, 100 consecutive measurements were recorded and the measured strain, SNR, bandwidth, strain gradient and precision are shown in Fig.6

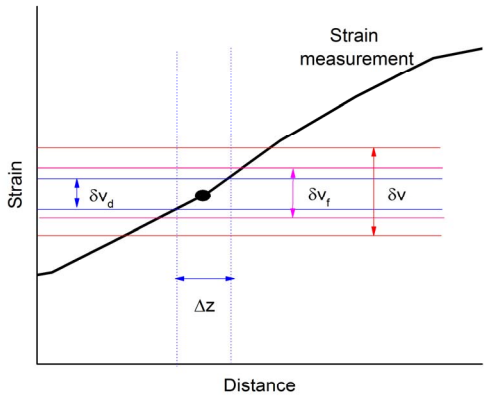

Figure 5 The relationship between distance resolution and precision error

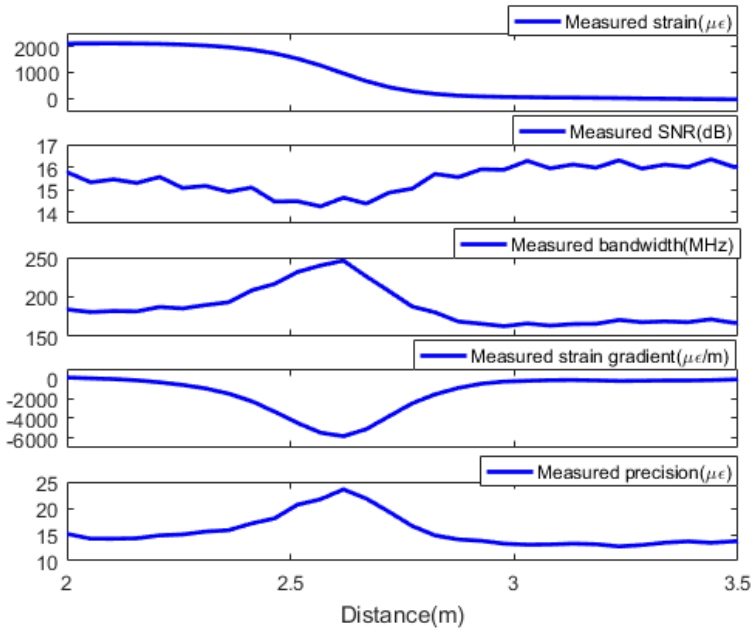

Figure 6 Analyzer measured strain, SNR, bandwidth, strain gradient, and measurement precision of a 2075 με step strain change

The frequency resolution induced error can be calculated by Eq. 1 with the measured SNR and bandwidth. The calculated frequency resolution induced error is shown in Fig. 7a. The maximum predicted frequency resolution is approximately 17 με at distance around 2.6m where the strain gradient is the largest, whereas the error is smaller at z=2-2.3m and z=3-3.5m where the strain gradients are smaller.

The distance resolution induced error is also calculated by the measured strain gradient, the timing error Δt (which is 9.4ps) and refractive index n (which is 1.5) using Eq. 5. The calculated error is shown in Fig. 7b. Near the largest strain gradient section z=2.6m, the distance resolution induced error increases rapidly from almost zero (at z=2-2.3m and z=3-3.5m) to about 17 με, indicating that the distance error is significantly affected by the strain gradient. When strain gradient is small, the distance error can be ignored.

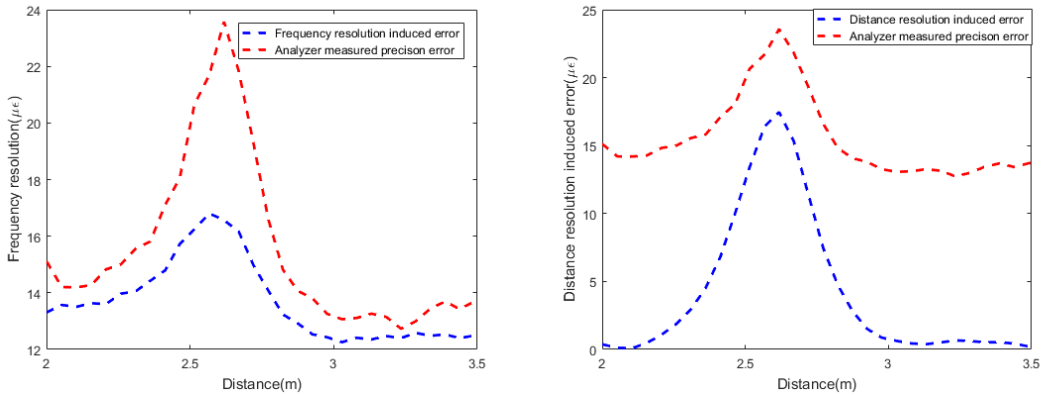

(a) (b)

Figure 7 (a) Comparison of the predicted frequency resolution induced precision error and the analyzer measured precision error; (b) Comparison of the predicted distance resolution induced precision error and the analyzer measured precision error

Fig. 8 shows the combination of the two errors by Eq. 2. At locations between x=2.5 m and 2.7 m, the strain changes rapidly. The strain gradient becomes maximum at x = 2.6 and both interrogator measured, and predicted precision errors become peak with about 24 με. In contrast the precision error at constant strain section is about 13-14 με. The difference between the simulated error and the interrogator measured error is less than 8% of the measured error. This finding is consistent with the previously published laboratory observations, where an extra repeatability error of 5 με was reported in a non-uniformly compressed beam where a load was applied to the middle of the beam [11].

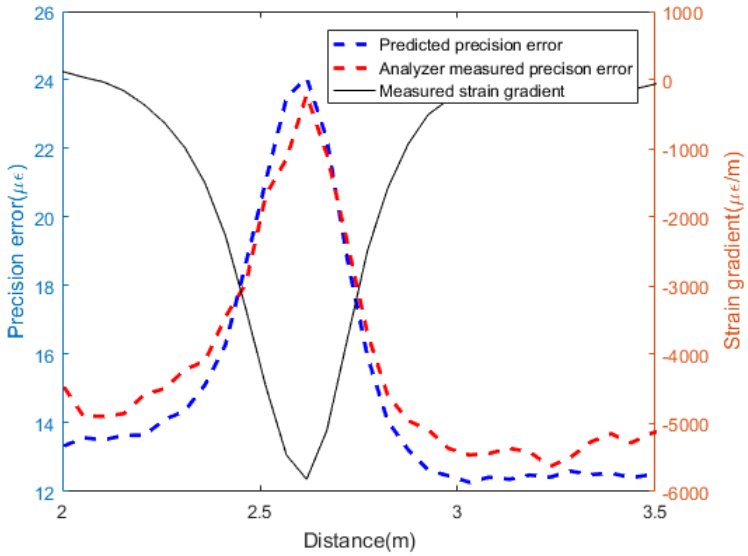

Figure 8 Comparison of the calculated precision error and the interrogator measured precision error for a step strain change input

4. Precision Error Correction

Because the SNR and bandwidth of a signal is determined by the interrogator, precision error cannot be corrected in the post-processing. The most direct way to minimize precision error is to increase the number of readings when the data is recorded. However, it is

unrealistic to take many readings, especially on a field site where temperature/strain condition can change with time. The previous section shows that strain gradient has large influence on distance resolution induced error. This section describes a distance error correction method using a sectional horizontal shift algorithm. This process improves the measurement precision for non-uniformly distributed strain cases. The reliability of the method is verified in the laboratory using measurements taken by a BOTDR interrogator.

4.1 Precision error correction method

Frequency resolution induced error is related to the properties of an interrogator, and can be minimized by optimizing the interrogator's parameters such as increasing averaging numbers, improving signal power, etc. Distance resolution induced error is caused by the unstable localization scheme of the interrogator, and its effect can be enlarged by non-uniformity of the strain distribution, as discussed earlier.

To correct for the distance error, a shift of strain measurement in the horizontal direction is proposed considering the localization error of the interrogator. Fig. 9 shows two repeated measurements (ε_r and ε). In structural health strain monitoring, the interest is the strain increment from the initial baseline reading. The emphasis for correction at large strain changing sections is because precision error is large when the strain gradient is large. As demonstrated in Fig. 9, the first strain reading ε_r is the reference strain and the subsequent reading ε is due to the localization error of the interrogator. Although there is no externally generated strain, the change in strain $\Delta\varepsilon$ is recorded. Herein, the strain profile ε needs to be corrected back by horizontally shifting with distance of Δz to minimize the sum of $\Delta\varepsilon$ along the measured section.

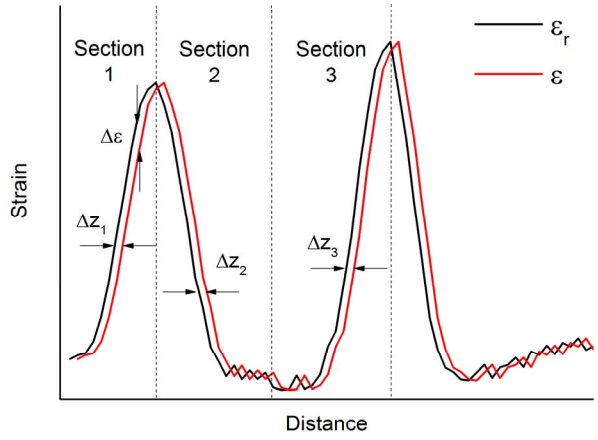

Figure 9 Illustration of distance resolution induced precision error correction method

Two ways to conduct horizontal shift are introduced here: (i) global shift and (ii) sectional shift. Global shift means that all measurements along the cable are shifted together to minimize the difference between ε_r and ε for the whole cable. Sectional shift means that measurements are separated into different sections based on strain gradient information (e.g., sections 1, 2 and 3 in Fig. 9) and sectioned strain data are horizontally shifted separately to minimize the difference between ε_r and ε in each section. The measured baseline strain profile is divided into sections based on the strain gradient

information; each section contains at least one large strain gradient data and has two end points with strain gradient close to zero.

To improve the accuracy of the horizontal shift, interpolation between measured points is necessary. Before any shift is applied, the data is interpolated 100 times to increase the shift accuracy. Initially the distance between each data is 5cm, after the interpolation, the data density becomes 0.5mm per data. All the data in the sectional shift section are then moved Δz to reduce the distance error. Δz is tested to be moved from -10cm to$+10\text{cm}$ and each time it moved 0.5mm. In total 400 points are tested.

The optimum horizontal shift Δz is determined by evaluating how much the repeated measurement has moved compared to the reference that represents the minimum difference between the two sets of data. The horizontal shifting process can be expressed as:

$$\text{Optimum}(\Delta z) \rightarrow \min \sum(\varepsilon(z_0 + \Delta z) - \varepsilon_r(z_0)) \quad (6)$$

where Δz is the horizontal shift, z_0 is the original location of the measuring point, ε is the strain value of the target data set, and ε_r is the strain reading of the reference data set.

The measurement distance error due to imprecise localization determination is randomly distributed along the cable length. Therefore, the distance error compensation method to horizontally shift the measurement should be done locally (i.e. sectional method). The performance difference between the global shift and sectional shift will be shown later on.

4.2 Precision error correction experimental verification

The horizontal shift method to minimize the measurement precision error was verified by a laboratory experiment. Fig. 10 illustrates the experimental set up where an optical fiber (Fujikura reinforced-ribbon cable) was glued all along the groove of a Glass Fiber Reinforced Polymer (GFRP) beam. The length of the beam is 4m, whereas the cross-sectional area is 7 mm×40 mm. The cross-sectional area of the tested cable is 1.3 mm×5 mm. The strain condition of the glued fiber sensor was control by different fixing positions. The beam attached with the fiber optic cable was placed with four or five fixing points as shown in Fig. 11 to hold and guide the bending deflection.

Figure 10 The bending beam test set up

The beam was bent in the following three conditions: (Case 1) symmetric bending, (Case 2) asymmetric bending and (Case 3) larger asymmetric bending (Fig. 11). For each bending case, 100 repeated measurements were recorded by NBX-5000 BOTDR interrogator for precision error evaluation. The experiment was conducted in a temperature-controlled room. The sectional/global horizontal shifts of the measurements were made to verify the reliability of the proposed precision error correction method.

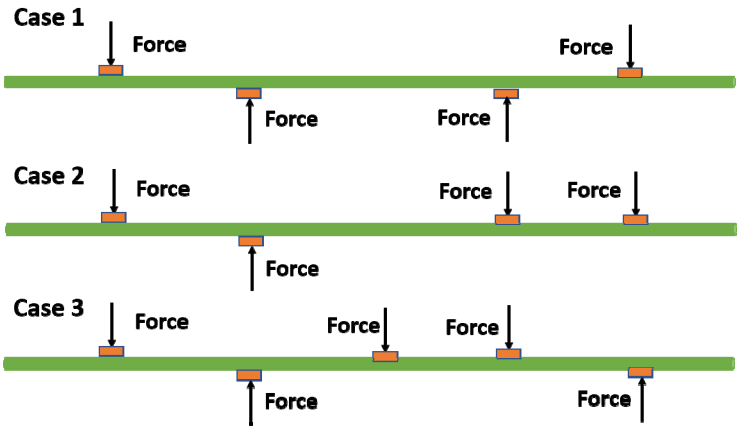

Figure 11 The three bending cases for the precision error correction method verification experiments

Fig. 12 shows the average strain profiles (black lines), the strain gradient profiles (blue lines) and the precision error profiles (red lines) for the three cases. Case 3 has the largest strain change at multiple locations, and its measurement precision error is the largest among the three cases. In Case 2, the precision error is large at large strain change sections. Case 1 does not show obvious precision error variations since the strain gradients are small; that is, the distance error is not significant compared to the interrogator random noise. The precision error of the most part of the tested beam is approximately 25με when the strain gradient is small. This 25με precision error is close to the value indicated in the datasheet of the interrogator. In Case 3, the strain gradients are large at around z = 2.6m and z = 3.3m and the precision errors (as much as 120με) are greater than the other locations due to the distance resolution induced error.

Fig. 13 shows the relationship between the measured precision error and strain gradient for the three cases. When the strain gradient is small or close to zero, the precision error is small and close to the accuracy listed on the interrogator datasheet. When strain gradient increases, the precision error increases especially when strain gradient is larger than 1000 με/m. This figure demonstrates that the relation between precision error and strain gradient. It verifies that the frequency resolution of the backscattered Brillouin spectrum and the distance resolution of the interrogator are the two important sources of the measurement precision error.

Based on the strain gradient and the strain value, the strain reading profile is separated into three sections (separated by the dashed lines in Fig.14a; z = 0−2.9m, z = 2.9m−4m and z = 4m−5m). As described earlier, the precision error correction is achieved in two different ways: global shift and sectional shift. Fig.14a and Fig. 14b compares the measurement precision error result without any corrections, and with the two correction processes. The globally horizontal shift reduces the measurement precision error from 120 με to 80 με at around x = 2.6m. However, at x = 3.5m−4.5m, the measurement precision error increases from 20 με to 80με. The sectional horizontal shift reduces the measurement precision error all along the cable, and the maximum error reduction reached is as large as 60με (at around x = 2.5m). Because the large strain gradient section in this experiment is short compared to the total fiber length, the error reduces at some locations but increases in the other sections in the global horizonal shift. The sectional horizontal shift reduces the

measurement precision error at most to 50% of its original error at large strain gradient sections.

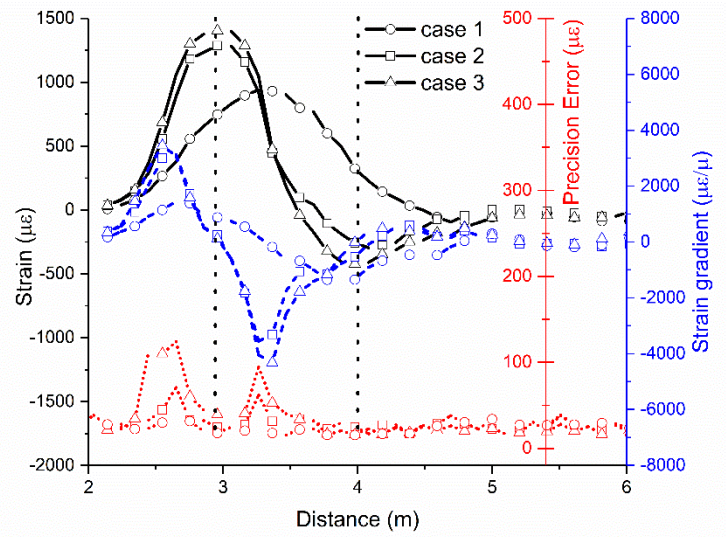

Figure 12 Measured strain, strain gradient and the corresponding precision error for three bending beam cases

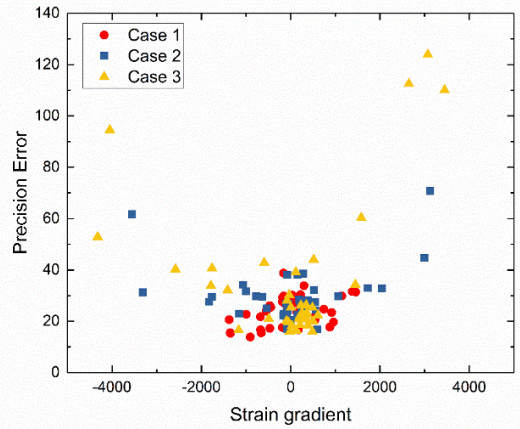

Figure 13 The precision error VS strain gradient plot on the case 3 fiber.

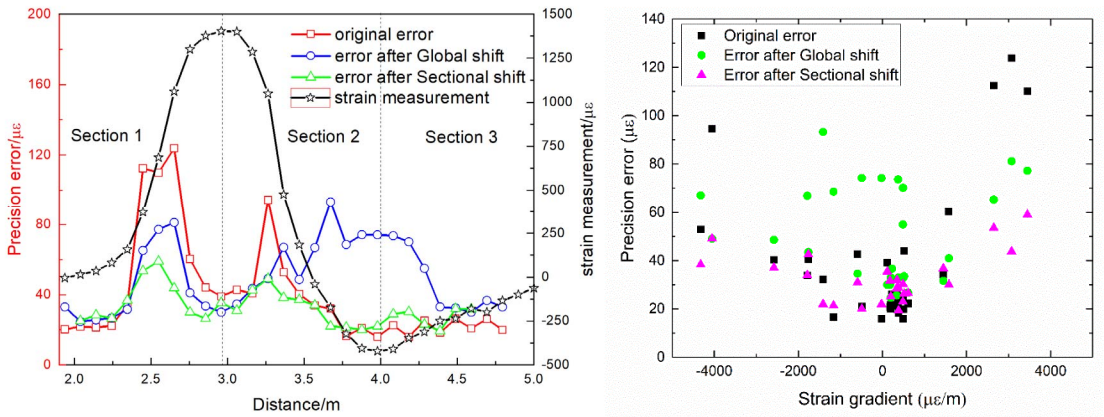

(a) (b)

Figure 14 Effects of the precision error compensation methods (a) the precision error profile before and after shift methods; (b) the precision error Versus Strain gradient plot before and after shift methods.

5. Field test pile monitoring case study

5.1 Field installation and measurements

The precision error compensation method described in Section 4 was applied to the data obtained from a full-scale load test of a reinforced concrete bored pile at a construction site in London, UK. The pile was 28.4 m deep and had a diameter of 0.9 m, as shown in Fig. 15a. This field test is described in more detail in another paper [21].

The pile cage, which had an outer diameter of 0.75 m, was instrumented with two different strain sensing fiber optic cables: a Fujikura JBT-03813 4-core cable and a Brugg (Solifos) V1 single core cable. A temperature sensing 4-core loose-tube Excel 205-300 fiber optic cable was also installed on the pile cage. All three cables were installed adjacent to each other, on the outside of the cage, in a single loop configuration, to provide the strain and temperature profiles on opposite sides of the pile (Fig. 15b). At the bottom of the cage, the cables looped around half the circumference of the cage. The strain cables were pre-tensioned before being fixed to the cage at approximately 0.6 m above the bottom and 1 m below the top of the cage. The instrumented reinforcement cage was inserted in the pile bore and concreted under bentonite support fluid. The individual cables exiting the pile head were then connected in series using fiber optic connectors, thus forming one complete circuit in the order Fujikura (strain) – Excel (temperature) – Brugg (strain). The Fujikura end of this circuit was connected to Neubrex BOTDR analyzer (NBX-5000) inside a nearby site office.

In preparation for the load test, a loading frame was built over the pile head and anchored to four anchor piles surrounding the test pile. The load test, which was carried out 45 days after the pile was concreted, consisted of applying a vertical, static load on the pile head in stages, during two loading-unloading cycles, while measuring the strain and displacement within the pile from the embedded fiber optic cables and other instrumentation. The measurements were used to investigate the pile shaft capacity and end capacity separately[22].

Measurements were taken at 10-minute intervals from the fiber optic cable circuit, with a sampling interval of 0.05 m, a spatial resolution of 0.50 m and an averaging count of 2^{16} readings. The analyzer was set to scan a frequency range of 10.2 to 11.1 GHz with a frequency step of 3 MHz. Before the load test, 270 measurements were taken from the fiber optic cables at rest during a 45-hour period. Subsequently, the load test lasted 87 hours.

The precision error analysis was carried out on the first 200 of the pre-load test measurements and on a minimum of 5 measurements from each of the load steps. The quality of the data was estimated from the strain gradient profile of the baseline raw data after concrete curing.

5.2 Precision error

Before the load test, 200 fiber optic strain data taking from Fujikura cable were recorded with no load applied and the last data in the data set was used as the baseline strain profile during loading steps. Fig. 16a shows the profiles of (a) averaged baseline strain ε, (b) Brillouin peak power, (c) bandwidth, (d) strain gradient ε', and (e) precision error along the test pile, from the top nearside to the top outside of the pile. The bottom of the pile was at about 49 meters. The strain was converted from the measured Brillouin frequency shift, using the calibrated strain coefficient (0.046MHz/με), and the precision error was calculated as the standard deviation of 200 measurement data sets. No strain change happened during that reading period because no load was applied to the pile. The baseline

strain profile was in a range of 0−2000με along the whole pile due to the installation effect. The peak power of the received signal varied between 153dB and 155dB. The power loss reached a maximum at distance z = 49m where the strain reduced sharply from 2000με to zero. The measured Brillouin spectrum bandwidth did not fluctuate significantly except at distance z=49m where the bandwidth achieves its maximum level of 200MHz. The measurement precision error significantly increased from 10με to 79με near distance z = 49m where the strain changes quickly. The strain gradient and its corresponding errors at each location on the fiber are shown in Fig. 16b. As expected, at location where the strain gradient changes significantly, the SNR drops, the bandwidth of the measured spectrum becomes wider, and the measurement precision error increases.

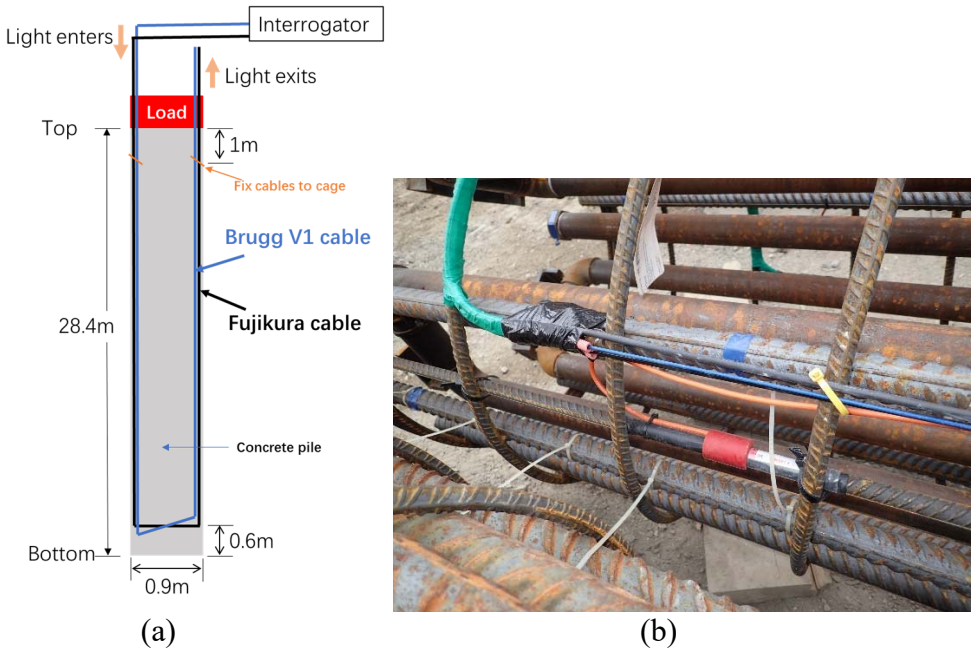

Figure 15 (a) The pile layout and fiber optic instrumentation in the field case. (b) The three fibre optic cables installed on the outside of the pile reinforcement cage, shown here attached near the bottom of the cage.

The frequency resolution is derived from the interrogator measured SNR and FWHM using Eq. 1. Fig. 17a compares the calculated frequency resolution induced precision error and the measured precision error. The measured precision error displays a varying precision error along the cable length, with a baseline of about 10με and a peak value as much as 79με. The baseline value is close to the uniform precision error indicated in the datasheet of the interrogator, attributed to the analyzer random noise. The calculated frequency resolution induced error stays at around 8με, while the measured error varies in a larger range and achieved to as much as 75με.

The distance resolution induced error is calculated using Eq. 5, with the laboratory calibrated timing error as 9.4 ps. Fig. 17b compares the calculated distance resolution induced error and the actual precision error profile. The calculated distance error is close to zero where there is little strain change, and it significantly increases where there is large strain gradient (at distance around z = 49m). A similar trend can be found in the actual precision error. In most parts of the cable, the calculated distance error varies in a range of 0−8με and the actual measured error is 8−15με. Compared to the calculated frequency

resolution, the calculated distance error induced precision error is significant when the strain gradient is large.

The measured precision error profile is compared to the profile of the combined frequency resolution induced error and the distance resolution induced error using Eq. 2. Fig. 18 shows the comparison between the calculated precision error and the measured precision error. In general, the calculated error matches with the actual error; the difference is only 5με.

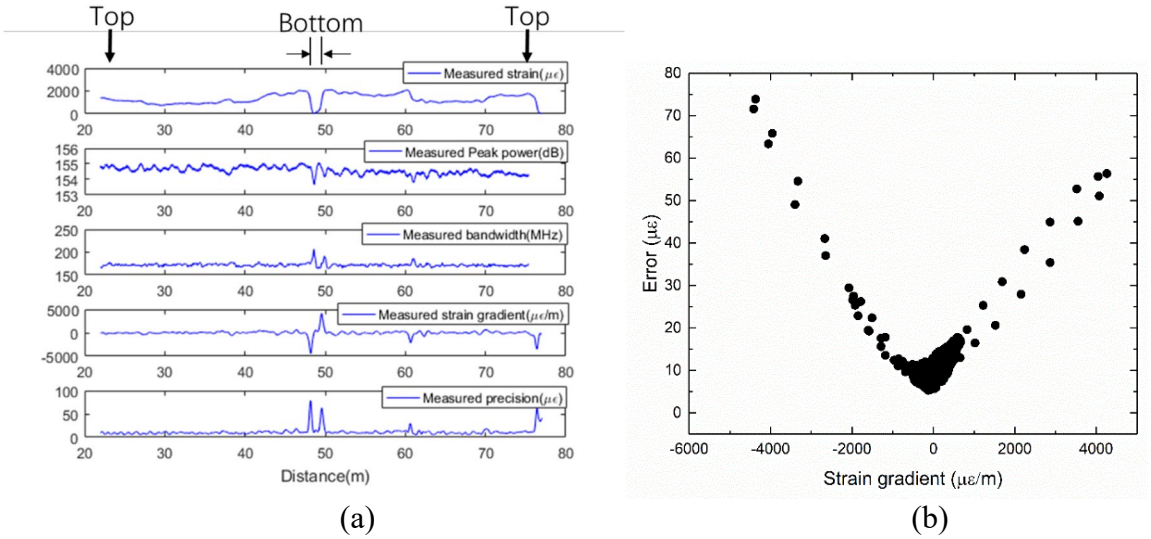

Figure 16 The measured 200 results of strain before loading. (a) The analyzer measured result including strain, peak power and bandwidth of the Brillouin spectrum, strain gradient and precision error. (b) The relationship between strain gradient and the measured errors in the readings.

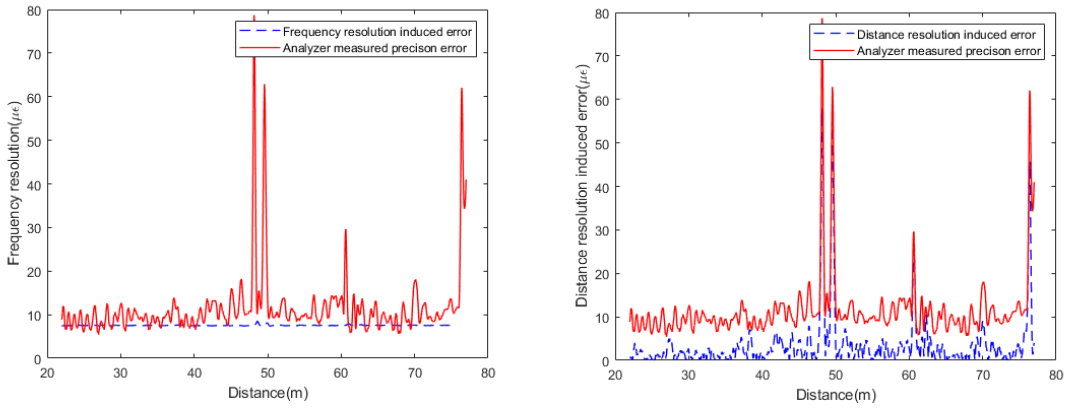

Figure 17 (a) The comparison of the analyzer measured precision error and the frequency resolution induced error calculated from the SNR and bandwidth of the Brillouin spectrum; (b) The comparison of the analyzer measured precision error and the distance resolution induced error calculated from the calibrated timing error of the analyzer

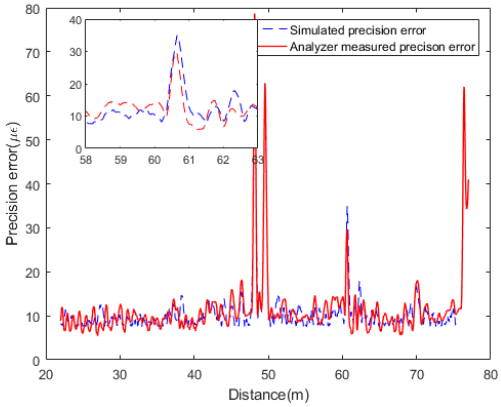

Figure 18 The comparison of the analyzer measured precision error and the predicted precision error compassion of the precision error at each distance

5.3 Loading data

During the load test, the strain response of the pile was measured by two fiber optic cables installed at same location: Fujikura reinforced strain sensing cable and the Brugg V1 strain sensing cable. In this paper, the performance of the two strain cables is not discussed, but the precision error generated by different strain gradients due to different pre-strain induced strain profiles of the two cables and the importance of uniform cable installation are discussed. The cables were installed parallel to each other; however, the two cables have different initial pre-strain profiles after the installation due to the manner the cables were attached to the cage. Therefore, the strain profile after the concrete was cured were different for these two cables.

Fig. 19 shows the BFS center frequency profiles of the two strain sensing cables at different load stages. The initial baseline strain profile of the Brugg strain cable was more variable that that of the Fujikura cable and therefore the initial strain gradient profiles are different. For both sensing cables, the general strain development trend and magnitude were in good agreement. The strain increment is close to zero at z = 48m and z=50m, where the bottom of the pile is located because the fiber there was placed perpendicular to the load direction and the fiber experienced very small strain.

The steps of loading and the measurements are shown in Fig. 20. First, before loading, continuous data was taken. Then, a load was applied to the pile. The load increased from 0% of the design load (DVL) to 100% and continued to 150% before it decreased to 0% again. Then the load was raised again to 200% before the weekend. During the weekend, the load was not changed. After the weekend, the test continued under 225% DVL and increased to 250% DVL. Finally, the load was released back to 0%. During the test, the load was remained unchanged while the interrogator was taking readings. For most load steps only a few readings were taken. However, more readings were taken at the following four loading stages: (i) 36 readings at 150% DVL, (ii) 31 readings in the subsequent 0% DVL, (iii) 160 readings at 200% DVL during the weekend, and (iv) 43 readings at 250% DVL. The readings were analyzed for the precision error evaluation and the horizontal shift method was applied to reduce the error.

Fig. 21a shows the precision error profile when the load is 150% DVL when 36 measurements were taken. The precision error increases where the strain gradient is large. The Fujikura cable has small strain gradient variation and hence the precision error is small.

The Brugg cable has some large strain gradients, leading to large precision error. When the strain gradient is within 1000 με/m, the precision error is close to the specification of the interrogator. The difference is mainly due to the pre-strain during the installation, as shown in Fig. 19. The baseline readings are more variable in the Brugg cable than in the Fujikura cable. This indicates large strain gradients in the initial strain profile for the Brugg cable and the timing error between the initial baseline reading and the readings in the load tests caused the fluctuations observed in the strain increment profiles.

Fig. 21b shows the strain gradient versus precision error for the two cables for the four datasets. The precision error before the load test shown in Fig.16b is also included for comparison. Results show that when the strain gradient is within 1000με/m, the precision error is close to 5-15 με, which is given in the datasheet of the interrogator. When the strain gradient increases, the precision error increases and reaches to about 80με for the Fujikura cable and 220με for the Brugg cable. The strain gradient is very large at some locations of the Brugg cable, and the precision error is as high as about 4000με.

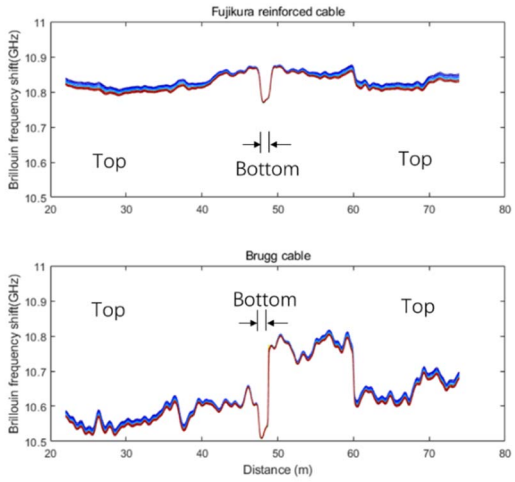

Figure 19 The center frequency profile of the two cables, the change of the profile is the result of different loading condition

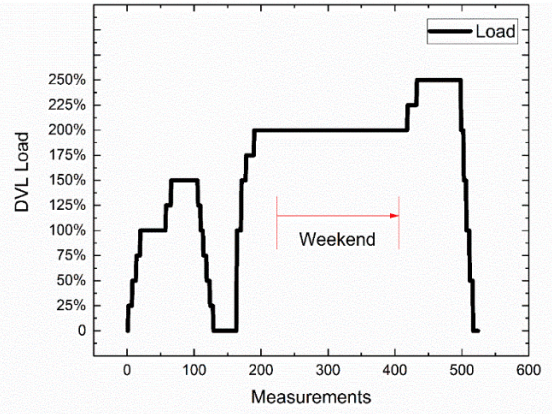

Figure 20 The load step during the loading test. Measurements are the readings recorded during the load test.

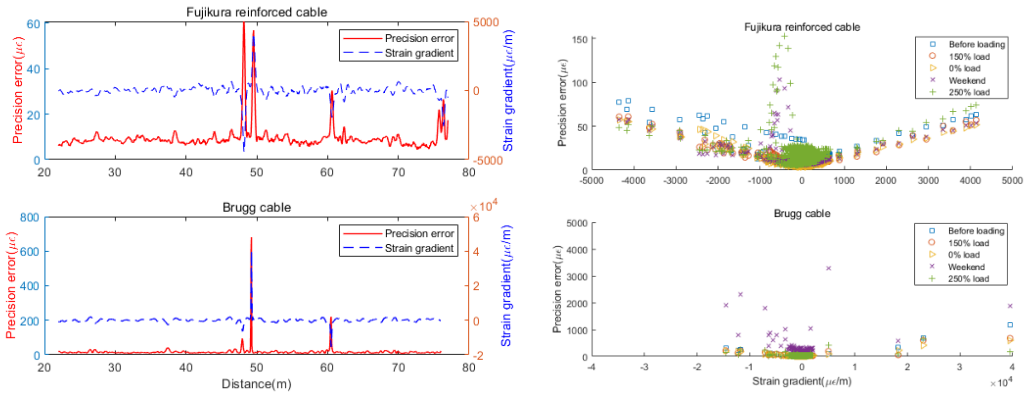

(a) (b)

Figure 21 (a) The precision error (red) and strain gradient (blue) profile at Fujikura and Brugg cable when load is 100% before horizontal shift. (b) The strain gradient VS precision error at Fujikura and Brugg cable

5.4 Improved strain profiles

In this section, the raw Brillouin center frequency profile is horizontally shifted to reduce the precision error. The two cables were installed at the same location but experienced different pre-strain, giving different initial Brillouin center frequency profiles, as shown by the red line in Fig. 22. The Brugg cable has large strain variation in the initial reading, indicating that it is expected to have large precision error.

Using the measured strain gradient σ_i' data of the initial baseline reading, the weights that represent the possibility of having large precision error are allocated to each measurement point using Eq. 7 [23].

$$\mathbf{W} = \max(\sigma_i') - \left\| \frac{\sigma_i' - mean(\sigma_i')}{std(\sigma_i')} \right\| \tag{7}$$

Fig. 22 shows the profiles of the calculated weights (blue line). Based on the weight profile, the horizontal shift sections are chosen, and they are marked as grey lines in the figure. The measurement data of the Fujikura cable are separated into seven sections, whereas that of the Brugg cable are separated into nine sections. In each section, the measurements are horizontally shifted to achieve the minimum distance resolution error between the baseline and subsequent readings.

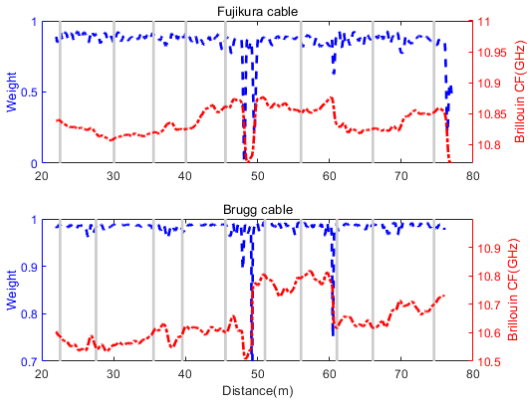

Figure 22 The initial reading before loading strain profile (red dash dot line), the weighted strain gradient (blue dash line), and the illustration of the data interpretation section (sections are divided by the grey solid lines) which is determined by the data weight profile for the field site load test

The results of the strain increment calculation, after horizontal shifting of the measured Brillouin center frequency in sections, are shown in Fig. 23. Compared to the raw precision error profile (Fig. 21a), the revised precision error reduces where the raw precision error was affected by the large strain gradient (Fig. 21a). The strain gradient versus precision error plots are shown in Fig. 24 for both cables. The precision errors are reduced at large strain gradient sections (>1000 με/m) and the reduced precision error is about 10 με, which is close to the specification of the interrogator. More specifically, at 1000 με/m, the original precision error was about 20 με while after the horizontal shift, the precision error was reduced to about 10 με. When the strain gradient is larger than 1000 με/m, the precision error increased when the strain gradient became larger in the original dataset. After the horizontal shift, the precision error became about 10 με, independent of strain gradient. In general, the precision error reduces at least 50% when the strain gradient is larger than 1000με/m.

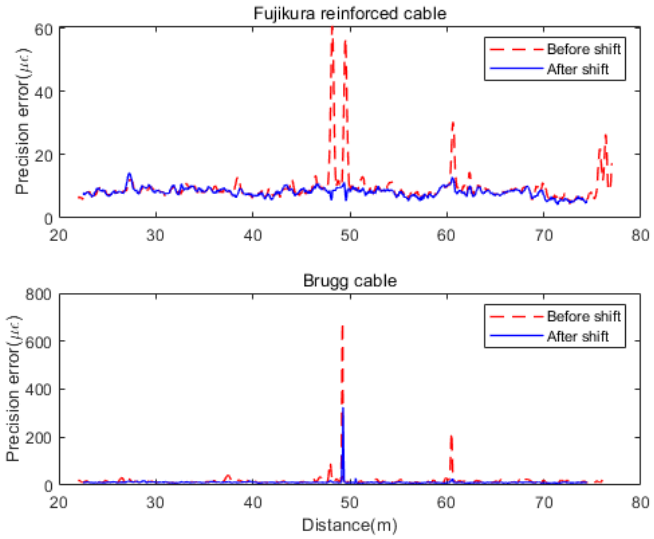

Figure 23 The precision error distribution before and after the horizontal shift.

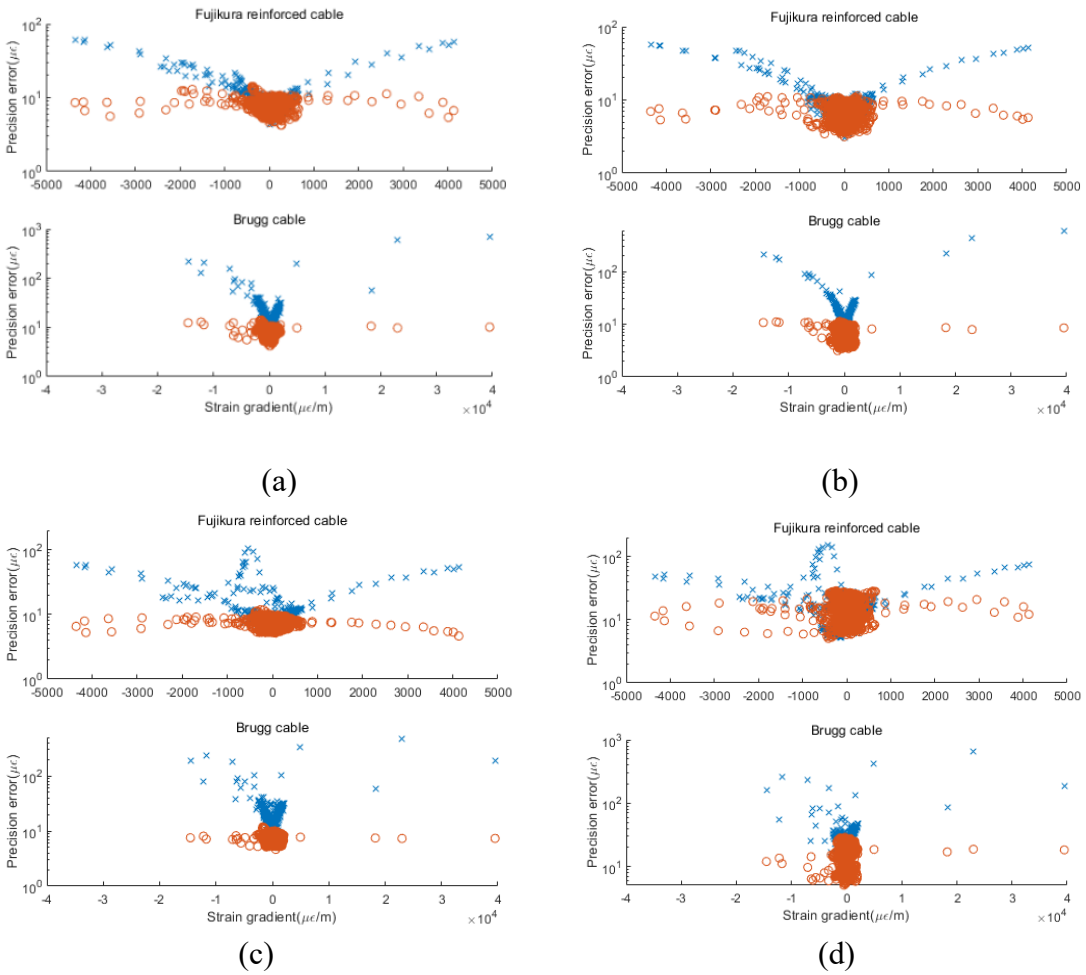

Figure 24 The precision error Versus strain gradient before (blue) and after (red) horizontal shift at load (a) 150%, (b) 0%, (c) weekend, (d) 250% DVL.

In this paper, it is noted the thermal variance induced precision error was ignored because of the small variance of temperature in the lab and pile loading environment. Further investigation is needed to examine how the overall precision error is affected by the reproducibility error that is generated when thermal compensation is conducted to the strain data. Furthermore, the strain transfer between structure and fiber is assumed to be excellent and stable with a tight coupling and bonding. The study hypothesizes that one of the causes of precision error originates from the measurement principle of the Brillouin strain sensing when the baseline strain profile is variable, which is caused during the sensor installation process. There are other causes of precision error (for example, imperfect strain transfer), which requires further investigation to examine their contributions to precision error.

6. Conclusions

Precision error in BOTDR strain measurement is the combination of (a) the frequency resolution induced error originated from the distorted Brillouin spectrum of non-uniform strain profile and (b) the distance resolution induced error of the interrogator. In this paper, a theoretical analysis shows that precision error increases at locations where there is large strain gradient, and this was confirmed by various laboratory experiments. The relationship between the degree of precision error and strain gradient was shown.

When a fiber optic sensing cable is attached or embedded into a structure, the installation process gives a non-zero initial strain profile. Poor quality of installation can lead to large spatial variation in the initial strain. When DFOS data with non-uniform initial strain profile are interpreted, strain gradient dependent precision error needs to be taken into consideration. The distance resolution induced precision error can be reduced by horizontally shifting the measurement in sections. In the laboratory test, the error was reduced from 120 με to 60 με, which is almost half of the original error. In the field pile loading case, the precision error did not significantly increase until the strain gradient was greater than 200 με/m. At the locations where the strain gradient is larger than 1000 με/m, the horizontal shift method decreased the precision error 50%.

It is considered that the proposed method is suitable for other structures or systems. In structural health monitoring application of distributed BOTDR strain measurement, the fiber optic sensing cable should be installed carefully so that the initial strain profile is as uniform as possible. After cable installation, every installation should conduct a precision error test on the baseline reading so that the quality of the installation can be evaluated by plotting the precision error-strain gradient relationship paper. A better quality of the strain increment data from the subsequent readings can be achieved by the data correction method describes in this paper.

Acknowledgements

The authors would like to acknowledge the contribution of Peter Knott in the installation of the test pile instrumentation. This field test pile monitoring case study was supported by UK EPSRC grant EP/N021614/1 and Innovate UK grant 920035.

Data access

The data obtained from the field test pile monitoring case study are commercially sensitive / confidential and therefore cannot be made publicly available.

Reference

1. Soga K, Luo L. Distributed fiber optics sensors for civil engineering infrastructure sensing. *J Struct Integr Maint*. 2018;3(1):1-21. doi:10.1080/24705314.2018.1426138
2. Lan C, Zhou Z, Ou J. Monitoring of structural prestress loss in RC beams by inner distributed Brillouin and fiber Bragg grating sensors on a single optical fiber. *Struct Control Heal Monit*. 2013;21(3):317-330. doi:10.1002/stc
3. Wang X, Shi B, Wei G, Chen SE, Zhu H, Wang T. Monitoring the behavior of segment joints in a shield tunnel using distributed fiber optic sensors. *Struct Control Heal Monit*. 2018;25(1):1-15. doi:10.1002/stc.2056
4. Song ZP, Zhang D, Shi B, Chen SE, Shen MF. Integrated distributed fiber optic sensing technology-based structural monitoring of the pound lock. *Struct Control Heal Monit*. 2017;24(7):1-8. doi:10.1002/stc.1954
5. Glisic B, Chen J, Hubbell D. Streicker Bridge: a comparison between Bragg-grating long-gauge strain and temperature sensors and Brillouin scattering-based

distributed strain and temperature sensors. In: Tomizuka M, ed. *Sensors and Smart Structures Technologies for Civil, Mechanical, and Aerospace Systems 2011*. Vol 7981. SPIE; 2011:674-683. doi:10.1117/12.881818

6. Yi T-H, Yao X-J, Qu C-X, Li H-N. Clustering Number Determination for Sparse Component Analysis during Output-Only Modal Identification. *J Eng Mech*. 2019;145(1):04018122. doi:10.1061/(asce)em.1943-7889.0001557

7. Chen G, Zhou Z, Xiao H, Huang Y. *Pilot Study on Rugged Fiber Optic Brillouin Sensors for Large-Strain Measurements to Ensure the Safety of Transportation Structures*. Vol Final Repo.; 2012.

8. Yu Y, Luo L, Li B, Soga K, Yan J. Frequency Resolution Quantification of Brillouin-Distributed Optical Fiber Sensors. *IEEE Photonics Technol Lett*. 2016;28(21):2367-2370. doi:10.1109/LPT.2016.2594084

9. Naruse H, Tateda M. Trade-off between the spatial and the frequency resolutions in measuring the power spectrum of the Brillouin backscattered light in an optical fiber. *Appl Opt*. 1999;38(31):6516. doi:10.1364/ao.38.006516

10. Mohamad H. Temperature and strain sensing techniques using Brillouin optical time domain reflectometry. *Smart Sens Phenomena, Technol Networks, Syst Integr 2012*. 2012;8346(March 2012):83461M. doi:10.1117/12.918329

11. Bao X, DeMerchant M, Brown A, Bremner T. Tensile and compressive strain measurement in the lab and field with the distributed Brillouin scattering sensor. *J Light Technol*. 2001;19(11):1698-1704. doi:10.1109/50.964070

12. Wu Z, Xu B, Hayashi K, Machida A. Fiber op-tic sensing of PC girder strengthened with prestressed PBOfiber sheets. In: Wu Z, Abe M, eds. *Proceedings of the First International Conference on Structural Health Monitor-Ing and Intelligent Infrastructures*. ; 2003:1191.

13. Hoepffner R. Distributed fiber optic strain sensing in hydraulic concrete and earth structures : measuring theory and field investigations on dams and landslides. 2008.

14. Hao Z, Zhishen W. Performance evaluation of BOTDR-based distributed fiber optic sensors for crack monitoring. *Struct Heal Monit*. 2008;7(2):143-156. doi:10.1177/1475921708089745

15. Luo L, Parmigiani F, Yu Y, Li B, Soga K, Yan J. Frequency uncertainty improvement in a STFT-BOTDR using highly nonlinear optical fibers. *Opt Express*. 2018;26(4):3870. doi:10.1364/oe.26.003870

16. Yamauchi Y, Co N, Neubrex K, Neubrex G. A study of the stability, reliability, and accuracy of neubrescope-based pipe thinning detection system. *SHMII-3 2007 3rd Int Conf Struct Heal Monit Intell Infrastruct*. 2007;(March).

17. Ji Y, Zou W, Long X, Chen J. Signal-to-noise ratio enhancement of stimulated Brillouin scattering based pulse compression of an ultrabroad microwave signal by use of a dispersion compensation fiber. *Opt Lett*. 2017;42(15):2980. doi:10.1364/ol.42.002980

18. Horiguchi T, Shimizu K, Kurashima T, Tateda M, Koyamada Y. Development of a Distributed Sensing Technique Using Brillouin Scattering. *J Light Technol*. 1995;13(7):1296-1302. doi:10.1109/50.400684

19. Soto MA, Thévenaz L. Modeling and evaluating the performance of Brillouin distributed optical fiber sensors. *Opt Express*. 2013;21(25):31347. doi:10.1364/oe.21.031347

20. Zhang D, Xu H, Shi B, Sui H, Wei G. Brillouin power spectrum analysis for partially uniformly strained optical fiber. *Opt Lasers Eng*. 2009;47(9):976-981. doi:10.1016/j.optlaseng.2009.04.008

21. de Battista N., Kechavarzi C, Seo H-J, Soga K, Pennington S. Distributed fibre optic sensors for measuring strain and temperature of cast-in-situ concrete test piles. In: *Proceedings of the International Conference on Smart Infrastructure and Construction (ICSIC)*. Cambridge; 2016.

22. Pelecanos L, Soga K, Elshafie MZEB, et al. Distributed Fiber Optic Sensing of Axially Loaded Bored Piles. *J Geotech Geoenvironmental Eng*. 2018;144(3):04017122. doi:10.1061/(asce)gt.1943-5606.0001843

23. Mei Y, Xu X, Luo L, Soga K. Reconstruction of Distributed Strain Profile Using a Weighted Spectrum Decomposition Algorithm for Brillouin Scattering Based Fiber Optic Sensor. *J Light Technol*. 2020;38(22):6385-6392. doi:10.1109/JLT.2020.3011686